The Shape of the K_α Line as a Possible Indication of the Black Hole Existence

A.F. Zakharov[1], S.V. Repin[2]
[1]*Institute of Theoretical and Experimental Physics, Moscow, Russia*
E-mail: zakharov@vitep5.itep.ru
[2]*Space Research Institute, Moscow, Russia*
E-mail: repin@mx.iki.rssi.ru

Observations of Seyfert galaxies in X-ray region reveal the wide emissive lines in their spectra, which can arise in inner parts of accretion disks, where the effects of General Relativity (GR) must be counted. A spectrum of a solitary emission line of a hot spot in Kerr accretion disk is simulated, depending on the radial coordinate r and the angular momentum $a = J/M$ of a black hole, under the assumption of equatorial circular motion of a hot spot. It is shown that the characteristic two-peak line profile with the sharp edges arises at a large distance, (about $r \approx (3 - 10)\ r_g$). The inner regions emit the line, which is observed with one maximum and extremely wide red wing. High accuracy future spectral observations, being carried out, could detect the angular momentum a of the black hole.

1 Introduction

The general status of black holes described in a number of papers (see, for example [1, 2, 3] and references therein). As it was emphasized in these reviews the most solid evidence for an existence of black holes comes from observations of some Seyfert galaxies because we need a strong gravitational field approximation to interpret these observational data, so probably we observe manifestations radiation processes from the vicinity of the black hole horizon (these regions are located inside the Schwarzschild black hole horizon, but outside the Kerr black hole horizon, thus we should conclude that we have manifestations of rotational black holes).

Recent observations of Seyfert galaxies in X-ray band [4, 5, 6, 7, 8, 9] reveal the existence of wide iron K_α line (6.4 keV) in their spectra along with a number of other weaker lines (Ne X, Si XIII,XIV, S XIV-XVI, Ar XVII,XVIII, Ca XIX, etc.). The line width corresponds to the velocity of the matter motion of tens of thousands kilometers per second, reaching the maximum value $v \approx 80000 - 100000$ km/s [5] for the galaxy MCG-6-30-15 and $v \approx 48000$ km/s [10] for MCG-5-23-16. In some cases the line has characteristic two-peak profile [5, 11] with a high "blue" maximum and the low "red" one and the long red wing, which gradually drops to the background level.

For individual objects, where the existence of the black holes is assumed, a strong variability of X-ray brightness was registered [12], as well as the rapid changes of the line profile (Yaqoob et al. [11], NGC 7413) and the quasiperiodic oscillations ([13], GRC 1915+105).

The large amount of observational data requires its comprehension, theoretical simulation and interpretation. The numerical simulations of the accretion disk spectrum under GR assumptions has been reported in the paper [14]. In the paper [15] the observational manifestations of GR effects are considered in X-ray binaries. Different physical models of the origin of a wide emissive iron K_α line in the nuclei of Seyfert galaxies are analyzed in the paper [16]. Non-geodesic motion of

the emitting hot spot, representing the magnetic field loop, is simulated in the paper [17] in the framework of the magnetohydrodynamics approach.

The numerical approach, applied here based on the method, described earlier in papers [18, 19, 20, 21].

2   The particles motion in a Kerr metric

Many astrophysical processes, where the great energy release is observed, are assumed to be connected with the black holes. Because the main part of the astronomical objects, such as the stars and galaxies, possesses the proper rotation, then there are no doubts that the black holes, both stellar and supermassive, possess the intrinsic proper rotation too.

The stationary black holes are described by the Kerr metric [22]:

$$
ds^2 = \quad -\frac{\Delta}{\rho^2}\left(dt - a\sin^2\theta d\phi\right)^2 +
$$

$$
+\frac{\sin^2\theta}{\rho^2}\left[\left(r^2 + a^2\right)d\phi - adt\right]^2 + \frac{\rho^2}{\Delta}dr^2 + \rho^2 d\theta^2, \tag{1}
$$

where

$$
\rho^2 = r^2 + a^2\cos^2\theta, \tag{2}
$$

$$
\Delta = r^2 - 2Mr + a^2. \tag{3}
$$

The photons trajectories can be described by the standard equations of geodesics:

$$
\frac{d^2 x^i}{d\lambda^2} + \Gamma^i_{kl}\frac{dx^k}{d\lambda}\frac{dx^l}{d\lambda} = 0, \tag{4}
$$

where Γ^i_{kl} are the Christoffel symbols. The equations however can be simplified if we will use the complete set of the first integrals which were found by Carter [23]: $E = p_t$ is the particle energy at infinity, $L_z = p_\phi$ is z-component of its angular momentum, $m = p_i p^i$ is the particle mass and Q is the Carter's separation constant [23]:

$$
Q = p_\theta^2 + \cos^2\theta\left[a^2\left(m^2 - E^2\right) + L_z^2/\sin^2\theta\right]. \tag{5}
$$

As shown by Zakharov [24, 18], the equations of photon motion can be reduced to

$$
\frac{dt'}{d\sigma} = -a\left(a\sin^2\theta - \xi\right) + \frac{r^2 + a^2}{\Delta}\left(r^2 + a^2 - \xi a\right), \tag{6}
$$

$$
\frac{dr}{d\sigma} = r_1, \tag{7}
$$

$$
\frac{dr_1}{d\sigma} = 2r^3 + \left(a^2 - \xi^2 - \eta\right)r + (a - \xi) + \eta, \tag{8}
$$

$$
\frac{d\theta}{d\sigma} = \theta_1, \tag{9}
$$

$$
\frac{d\theta_1}{d\sigma} = \cos\theta\left(\frac{\xi^2}{\sin^3\theta} - a^2\sin\theta\right), \tag{10}
$$

$$
\frac{d\phi}{d\sigma} = -\left(a - \frac{\xi}{\sin^2\theta}\right) + \frac{a}{\Delta}\left(r^2 + a^2 - \xi a\right), \tag{11}
$$

where $\eta = Q/M^2 E^2$ and $\xi = L_z/ME$ are the Chandrasekhar's constants [25], which should be derived from the initial conditions in the disk plane; r and a are the appropriate dimensionless variables. The system (6)-(11) has also two integrals,

$$
\begin{aligned}
\epsilon_1 \quad &\equiv \quad r_1^2 - r^4 - \left(a^2 - \xi^2 - \eta\right) r^2 - \\
&\quad - 2 \left[(a - \xi)^2 + \eta\right] r + a^2 \eta = 0,
\end{aligned}
\tag{12}
$$

$$
\epsilon_2 \quad \equiv \quad \theta_1^2 - \eta - \cos^2 \theta \left(a^2 - \frac{\xi^2}{\sin^2 \theta}\right) = 0,
\tag{13}
$$

which can be used for the precision control. This method differs from the approach which was developed in papers [26, 27, 28, 29].

3   Numerical method

We assume that the hot spot emits isotropically distributed quanta in the local frame. First, one should define the Chandrasekhar's constants for each quantum and then integrate the system (6)-(11) to either the infinity or the events horizon, depending on the constants values.

The trajectories classification, depending on the Chandrasekhar's constants can be found in the papers [30, 31]. The integration procedure was made using the combination of 5-order Gear [32] and 12-order Adams methods, realized by Hiebert and Shampine [33]; Hindmarsh [34]; Petzold [35] for single precision and freely distributed in Internet. The original program has however been adapted for a double Pentium precision. The details of simulation and initial conditions can be found in papers [18, 21].

4   Simulation results

The simulated spectrum of a hot spot for $a = 0.9$, $\theta = 60°$ and different radius values is shown in Fig. 1. The proper quantum energy (in co-moving frame) is set to unity. The observer at infinity registers then the characteristic two-peak profile, where the "blue" peak is higher than the "red" one and the center is shifted to the left. Some spectrum jugging near its minimum is explained by pure statistical reasons and has no the physical nature.

As far as the radius diminishes the spectrum is enhanced, i.e. increases the residual between the maximum and minimum quanta energy, registered by far observer. For example, for $a = 0.9$, $r = 1.2 r_g$ and $\theta = 60°$, where r_g has its standard form $r_g = 2kM/c^2$, i.e. in the vicinity of the marginally stable orbit, the quanta, flown out to the distant observer, may differ 5 times in their energy. The red maximum decreases its height with diminishing the radius and at $r < 2 r_g$ becomes almost undistinguishable. It is interesting to note that the spectrum has very sharp edges, both red and blue. Thus, for $a = 0.9$, $r = 3 r_g$, $\theta = 60°$ the distant observer has registered 1433 quanta of 20417 isotropically emitted; 127 of them ($\approx 9\%$) drop to the interval $1.184 < E < 1.202$ (blue maximum) and 43 quanta drop to $0.525 < E < 0.533$ (red maximum), whereas no one quantum has the energy $E < 0.518$ or $E > 1.236$.

A spectrum of a hot spot for $a = 0.9$, $r = 1.5 r_g$ and different θ values is shown on Fig. 2. The spectrum for $\theta = 60°$ and the same a and r values is included in Fig. 1 and should be added to the current figure too. As it follows from the figure, the spectrum critically depends on the disk inclination angle. For large θ values, when the line of sight slips almost along the disk plane, the spectrum is strongly stretched, its red maximum is essentially absent, but the blue one appears narrow and very high. The red wing is strongly stretched because of the Doppler effect, so that the

observer registers the quanta with 5 times energy difference. As far as the θ angle diminishes the spectrum grows narrow and changes the shape: its red maximum first appears and then gradually increases its height. At $\theta = 0°$ both maxima merge to each other and the spectrum looks like the δ-function. It is evident since all the points of the emitting ring are equal in their conditions with respect to the observer. The frequency of registered quanta in that case is 2 time lower than the frequency of the emitted ones. A fall in frequency consists here in two effects, acting in the same direction: the transversal Doppler effect and the gravitational red shift.
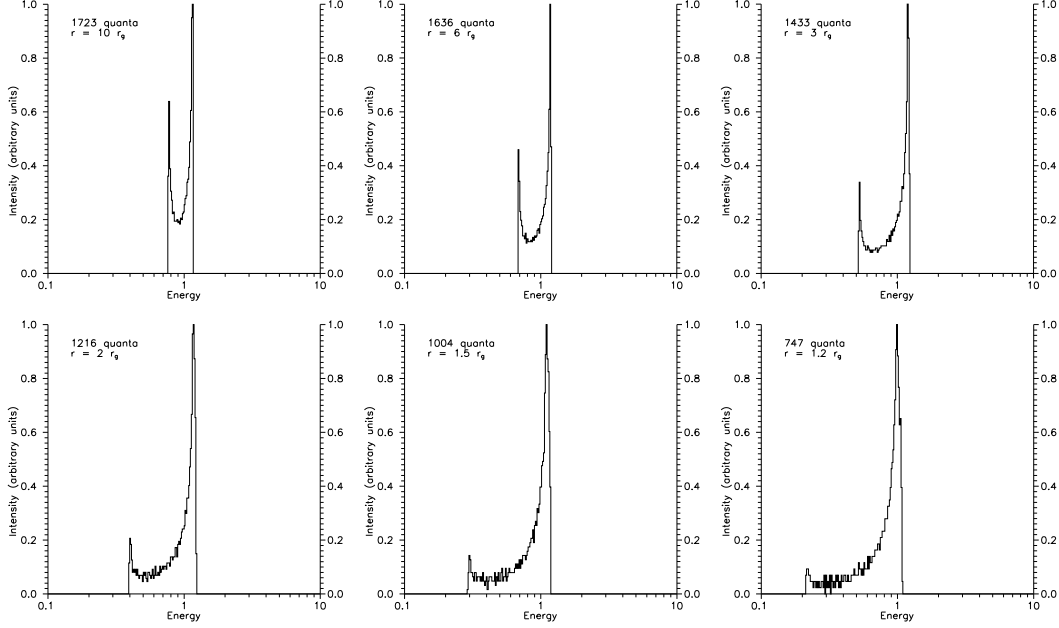
Fig. 1.   Spectrum of a hot spot for $a = 0.9$, $\theta = 60°$ and different values of the radial coordinate. The marginally stable orbit lays at $r = 1.16r_g$.
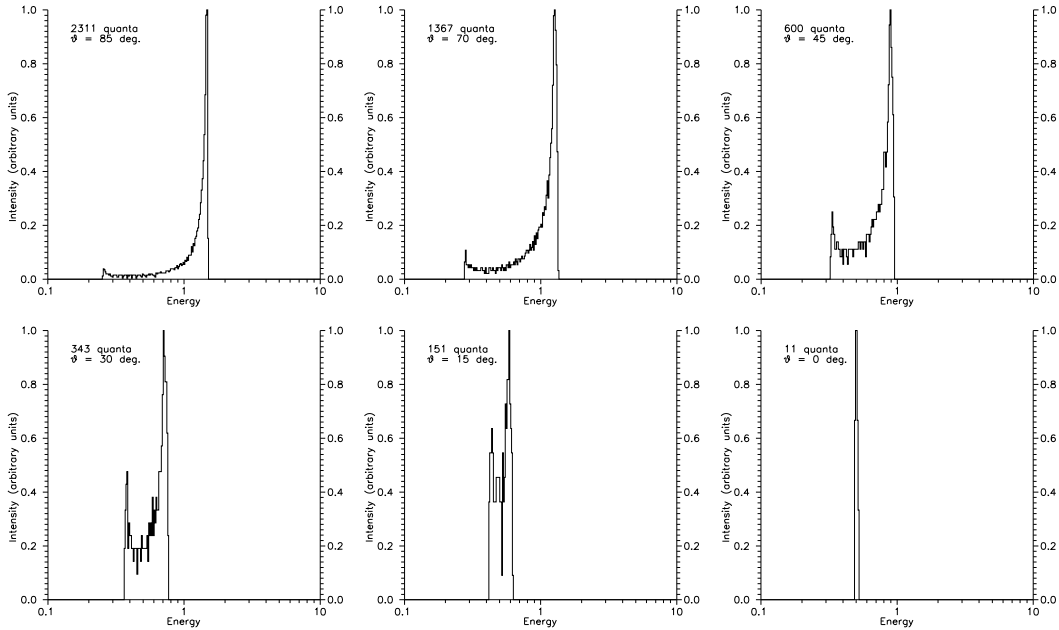

Fig. 2.   Spectrum of a hot spot for $a = 0.9$, $r = 1.5r_g$ and different θ angle values.

102
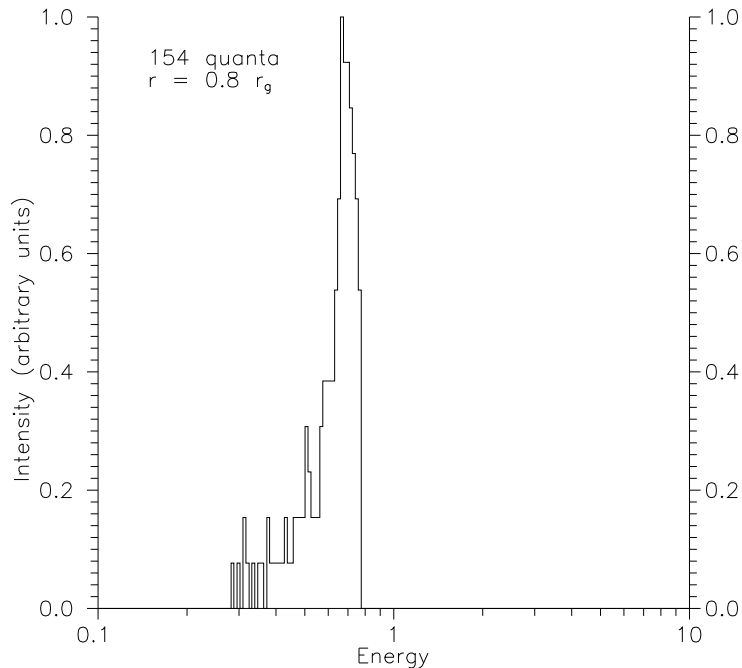
Fig. 3.   Spectrum of a hot spot for $a = 0.99$, $r = 0.8r_g$ and $\theta = 60°$.

Spectrum of a hot spot for $a = 0.99$, $r = 0.8r_g$, $\theta = 60°$ is shown on Fig. 3. The existence of a deep stable orbit ($r_{\min} = 0.727r_g$) leads to some new spectrum features. Thus, at $r \leq r_g$ the red maximum totally vanishes and the blue one is so shifted to red direction, that its frequency becomes less that unity. It is a pure manifestation of a GR gravitational red shift. The spot has a sharp blue edge ($E_{\max} = 0.69$, 45 quanta with $0.681 < E < 0.736$ and no one quantum with $E > 0.77$) and strongly loses its lustre (154 quanta total), because the main part of emitted quanta is captured by a black hole and only a small part, strongly red shifted, flies out to the observer. It is also noticeable that at $r = 0.8r_g$ the spectrum is heavily grown narrow. Indeed, it should be that, because for the orbit, laying nearby the horizon, there is quite a narrow cone in which the quanta can fly out to infinity.

5   Discussion and conclusions

The strong variability of Seyfert galaxies in X-ray does not contradict the assumption, that we observe the emission of the hot spots from the inner region of accretion disk, which can decay or grow dim, going towards a horizon as time passes. The spectrum dynamics is understood qualitatively by reference to Fig. 1,3, considered sequentially from top to bottom. The exact time characteristics of this process depend critically on the disk model [36, 37] and on the physical nature of a hot spot and are not discussed here.

The assumption can be checked out in long-term systematic X-ray observations with high time resolution of such Seyfert galaxies as NGC 1068, NCG 2110, MCG-6-30-15, NGC 4507, etc., where K_α line is sharply defined. The observations could confirm the existence of multiple spots, which motion and dynamics lead to X-ray variability in intensity and spectrum.

References

[1] Zakharov, A.F. in Proceedings of the XXIII Workshop on High Energy Physics and Field Theory, 2000, p. 169.

[2] Frolov V.P., Novikov I.D. Physics - Uspekhi, 2001, **44**, 291.

[3] Liang E.P. Physics Reports, 1998, **302**, 69.

[4] Fabian, A.C., Nandra, K., Reynolds, C.S., Brandt, W.N., Otani, C., Tanaka, Y., Inoue, H., Iwasawa, K. MNRAS, 1995, **277**, L11.

[5] Tanaka, Y., Nandra, K., Fabian A.C., Inoue, H., Otani, C., Donati, T., Hayashida, K., Iwasawa, K., Kii, T., Kunieda, H., Makino, F., Matsuoka, M. Nature, 1995, **375**, 659.

[6] Nandra, K., George, I.M., Mushotzky, R.F., Turner, T.J., Yaqoob, T. ApJ, 1997a, **476**, 70.

[7] Nandra, K., George, I.M., Mushotzky, R.F., Turner, T.J., Yaqoob, T. ApJ, 1997b, **477**, 602.

[8] Malizia, A., Bassani, L., Stephen, J.B., Malaguti, G., Palumbo G.G.C. ApJSS, 1997, **113**, 311.

[9] Sambruna, R.M., George, I.M., Mushotsky, R.F., Nandra, K., Turner, T.J. ApJ, 1998, **495**, 749.

[10] Weawer, K.A., Krolik, J.H., Pier, E.A. ApJ, 1998, **498**, 213 (astro-ph/9712035).

[11] Yaqoob, T., McKernan, B., Ptak, A., Nandra, K., Serlemitsos, P.J. ApJ, 1997a, **490**, L25.

[12] Sulentic, J.W., Marziani, P., Calvani, M. ApJ, 1998b, **497**, L65.

[13] Paul, B., Agrawal, P.C., Rao, A.R., Vahia, M.N., Yadav, J.S., Seetha, S., Kasturirangam, K. ApJ, 1998, **492**, L63.

[14] Bromley, B.C., Chen, K., Miller, W.A. ApJ, 1997, **475**, 57.

[15] Cui, W., Zhang, S.N., Chen, W. ApJ, 1998, **492**, L53.

[16] Sulentic, J.W., Marziani, P., Zwitter, T., Calvani, M., Dultzin-Hacyan, D. ApJ, 1998, **501**, 54.

[17] Romanova, M.M., Ustyugova, G.V., Koldoba, A.V., Chechetkin, V.M., Lovelace R.V.E. ApJ, 1998, **500**, 703.

[18] Zakharov, A.F. MNRAS, 1994, **269**, 283.

[19] Zakharov, A.F. 1993, Preprint MPA **755**.

[20] Zakharov, A.F. Annals for the 17th Texas Symposium on Relativistic Astrophysics, The New York Academy of Sciences, 1995, **759**, 550.

[21] Zakharov A.F., Repin S.V. AZh, 1999, **76**, 803.

[22] Misner, C.W., Thorne, K.S., Wheeler, J.A. Gravitation. W.H.Freeman and Company, San Francisco, 1973.

[23] Carter, B. Phys. Rev. D, 1968, **174**, 1559.

[24] Zakharov, A.F. AZh, 1991, **35**, 145.

[25] Chandrasekhar, S. Mathematical Theory of Black Holes. Clarendon Press, Oxford, 1983.

[26] Cunningham, C.T. ApJ, 1975, **202**, 788.

[27] Cunningham, C.T., Bardeen, J.M. ApJ, 1973, **183**, 237.

[28] Karas, V., Vokrouhlický, D., Polnarev, A.G. MNRAS, 1992, **259**, 569.

[29] Rauch, K.P., Blandford, R.D. Caltech Preprint, 1993, GRP-334.

[30] Zakharov, A.F. ZhETPh, 1986, **91**, 3.

[31] Zakharov, A.F. ZhETPh, 1989, **95**, 385.

[32] Gear, C.W. Numerical Initial Value Problems in Ordinary Differential Equations. Prentice Hall, Englewood Cliffs, NY, 1971.

[33] Hiebert, K.L., Shampine, L.F. Implicitly Defined Output Points for Solutions of ODE-s. Sandia report sand80–0180, February, 1980.

[34] Hindmarsh, A.C. ODEpack, a systematized collection of ODE solvers. In Scientific Computing. Stepleman, R.S. et al. (eds.), North–Holland, Amsterdam, 1983, pp. 55–64.

[35] Petzold, L.R. SIAM J. Sci. Stat. Comput., 1983, **4**, 136.

[36] Novikov, I.D., Thorne, K.S. in Black Holes, 1973, ed. C.DeWitt & B.S.DeWitt (New York: Gordon & Breach), 334.

[37] Shakura, N.I., Sunyaev, R.A. A&A, 1973, **24**, 337.